Figure S1

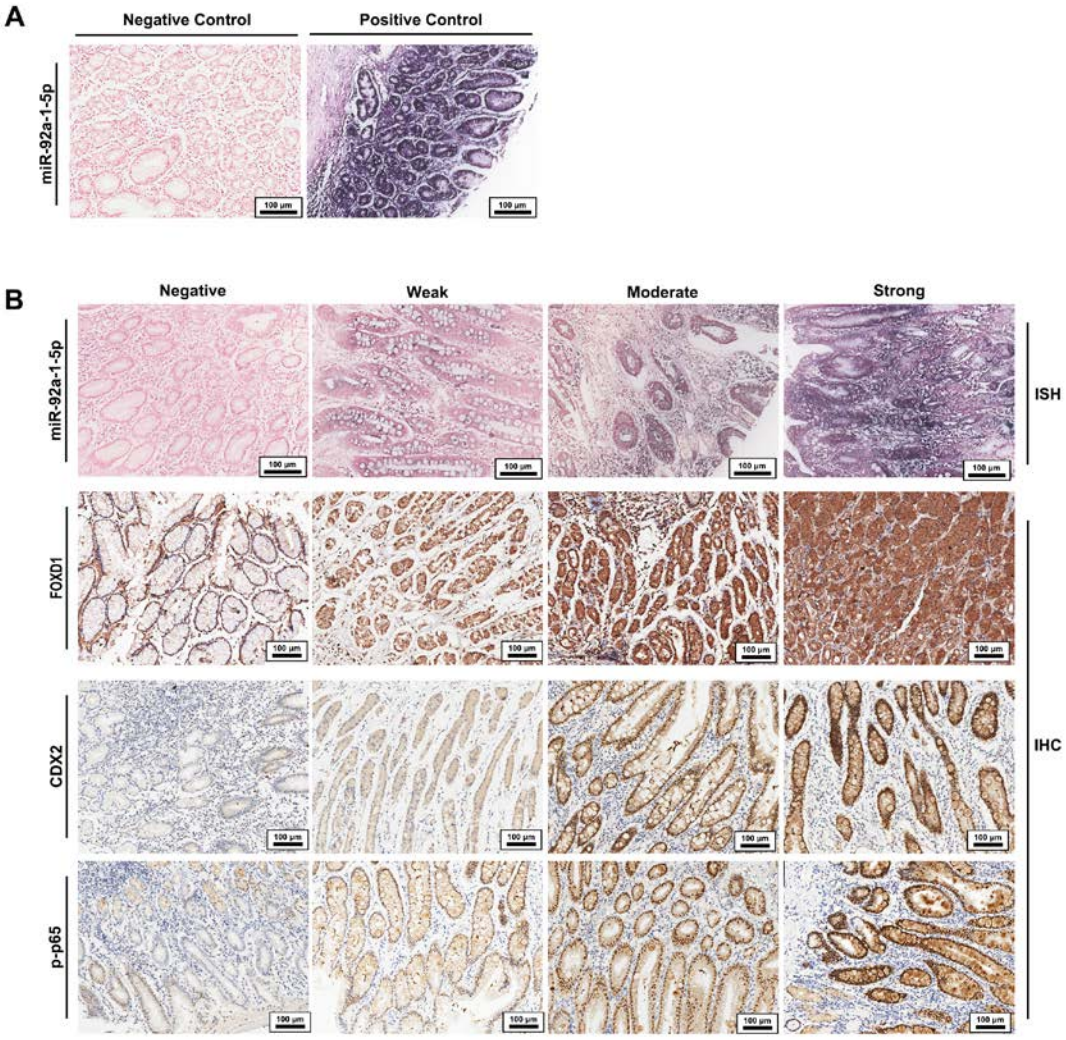

Supplemental Figure S1 Representative Images of ISH and IHC with different intensity.

(A) ISH were performed in IM tissues with LNA-modified and 5'- and 3'-DIG-labeled oligonucleotide probes. Positive control: U6 snRNA. Negative control: scrambled miRNA control. (B) Representative Images of ISH and IHC with different intensity of miR-92a-1-5p, FOXD1, CDX2 and p-p65. The intensity of staining was divided into four grades (intensity scores): negative (0), weak (1), moderate (2) and strong (3) and used in the calculation of histological score (Supplementary Materials and Methods).

Figure S2

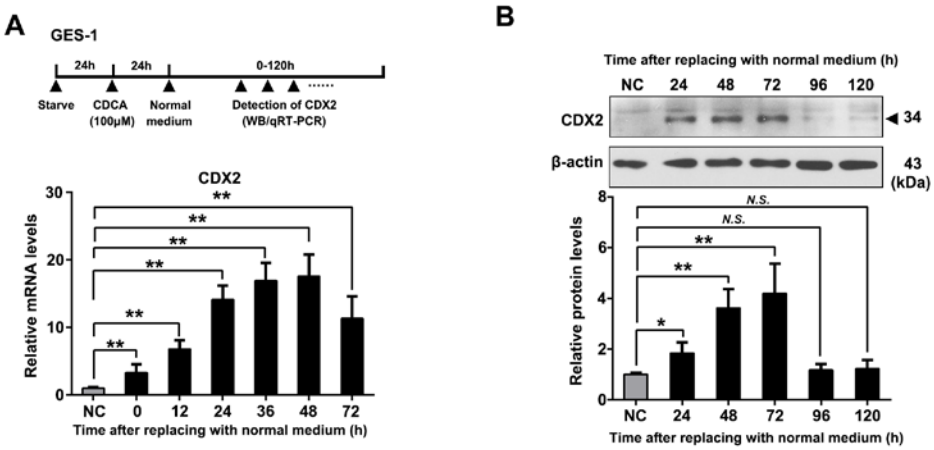

Supplemental Figure S2 CDX2 expression at different time points after ending of bile acids stimulation.

(A) Top: Workflow in this figure. GES-1 cells were treated with CDCA (100μM) for 24h after 24h starvation. The expression of CDX2 were detected at different time points after replacing with normal medium. Bottom: qRT-PCR results of CDX2 expression at different time points after replacing with normal medium. GAPDH RNA was used as internal control. (B) Top: Representative images of western blotting of CDX2 at different time points after replacing with normal medium. β-actin levels were used as internal control in immunoblots. Bottom: quantification of immunoblots normalized as to β-actin. Means ± SEM of a representative experiment (n = 3) performed in triplicates are shown.*, $P < 0.05$; **, $P < 0.01$.

Figure S3

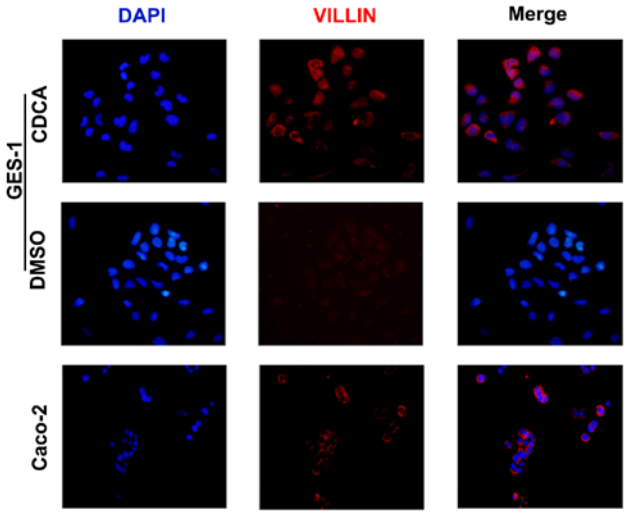

Supplemental Figure S3 Bile acids induced VIL1 expression in GES-1 cells.

Immunofluorescence showed VIL1 expression in GES-1 cells treated with CDCA (100 μM) for 24h. HT-29 as a positive control. Representative images in one of three independent experiments are shown.

Figure S4

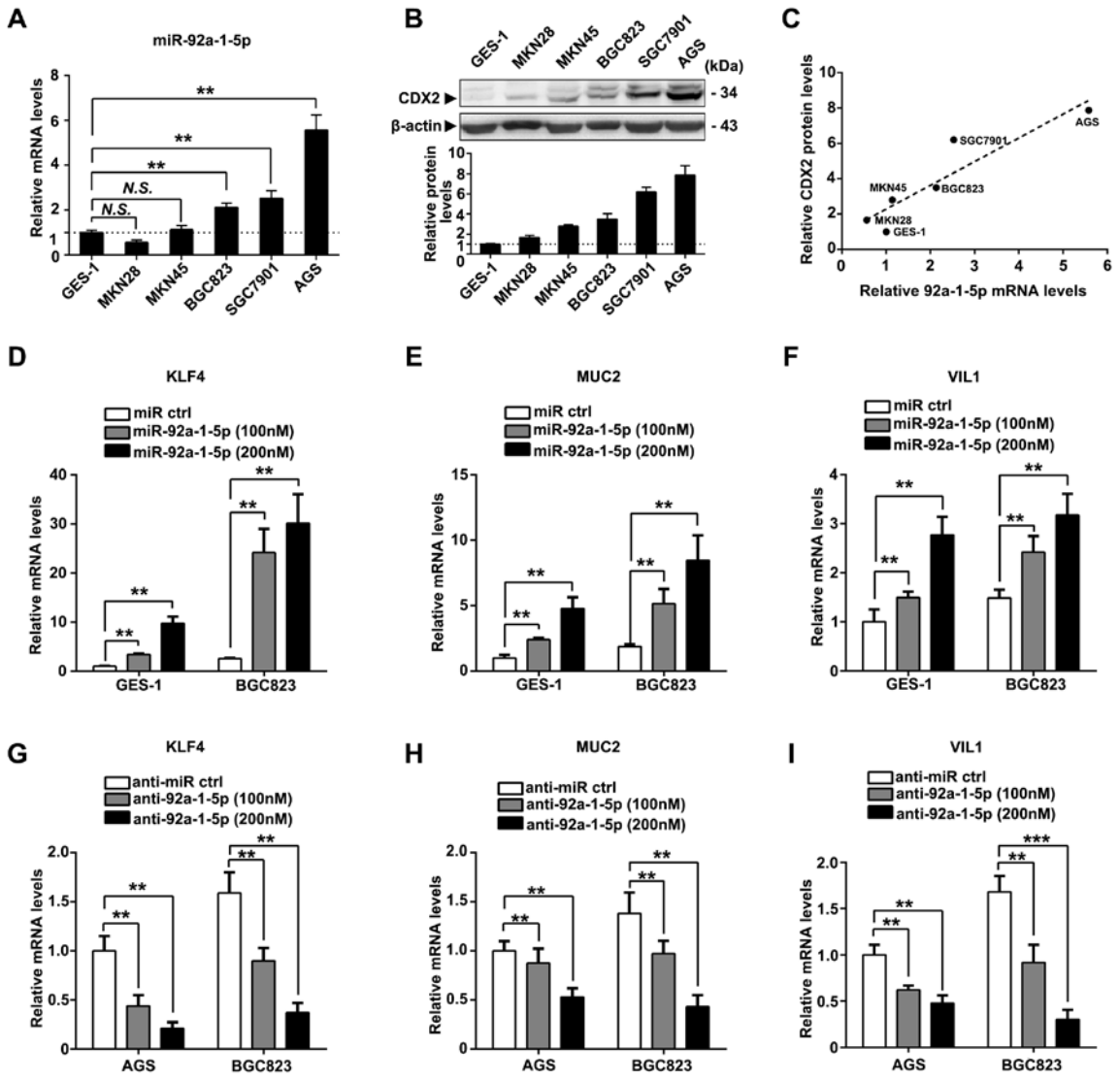

Supplemental Figure S4 miR-92a-1-5p increases KLF4, MUC2 and VIL1 expression in gastric cells.

(A) qRT-PCR results of miR-92a-1-5p in GES-1 and GC cell lines normalized as to expression of U6. (B) Western blot for CDX2 in indicated cell lines normalized as to expression of β-actin. (C) A positive correlation between levels of CDX2 and miR-92a-1- 5p in gastric cell lines. (D-F) GES-1 and BGC823 cells were transfected as in Fig. 3A and qRT-PCR were used to examine the expression of KLF4 (D) MUC2 (E) and VIL1 (F). (G-I) AGS and BGC823 cells were transfected as in Fig. 3B and qRT-PCR were used to examine the expression of KLF4 (G) MUC2 (H) and VIL1 (I). GAPDH RNA was used as internal control Means ± SEM of a representative experiment (n = 3) performed in triplicates are shown.*, $P < 0.05$; **, $P < 0.01$.

Figure S5

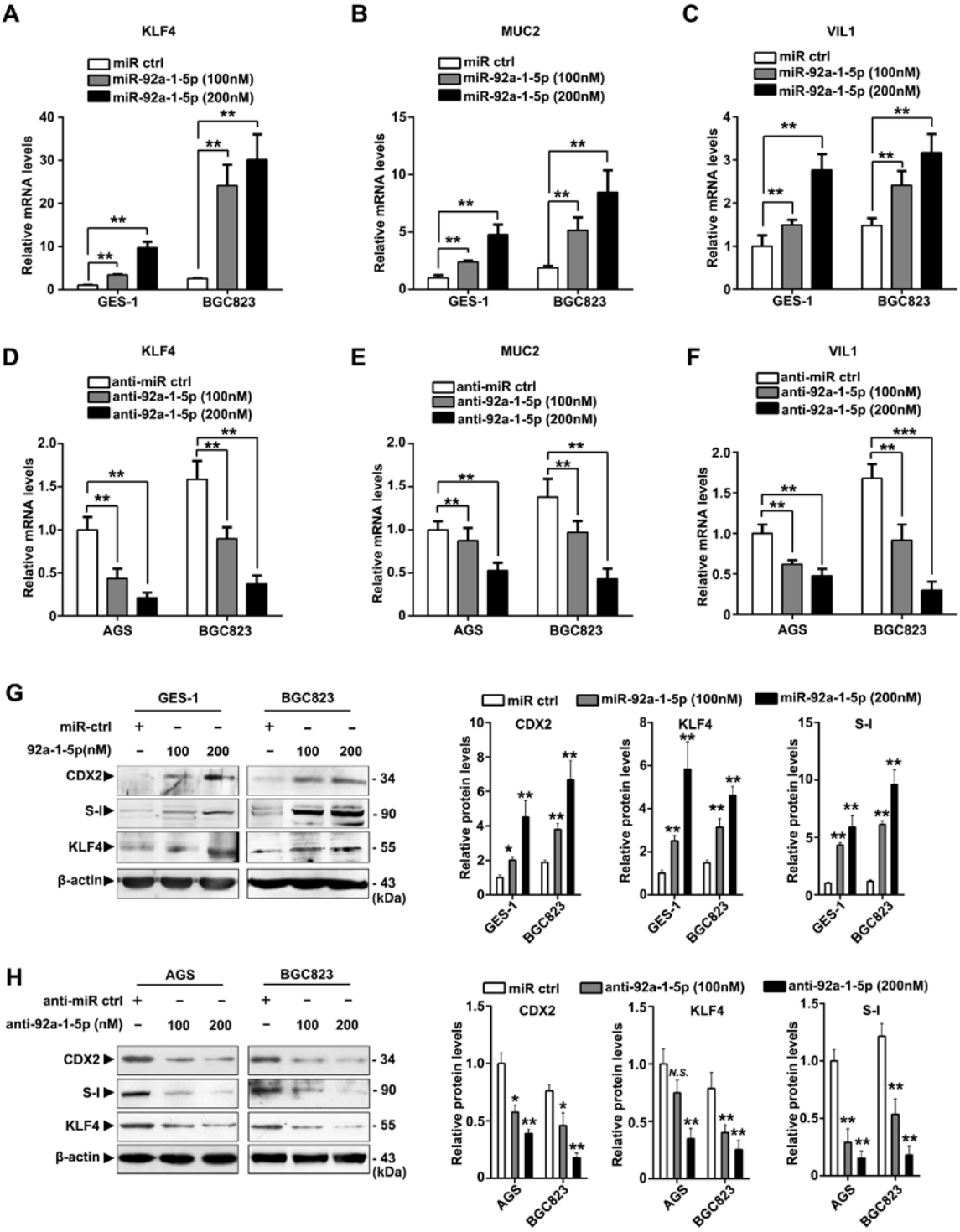

Supplemental Figure S5 miR-92a-1-5p increases KLF4, MUC2 and VIL1 expression in gastric cells.

(A-F) GES-1, AGS and BGC823 cells were transfected as in Fig. 3A and qRT-PCR were used to examine the expression of KLF4, MUC2 and VIL1. GAPDH RNA was used as internal control. (G) Left: Representative images of western blotting for CDX2, S-I and KLF4 in GES-1 and BGC823 cells transfected as in Fig. 3A top. Right: Quantification of protein levels of CDX2, S-I and KLF4 respectively. (H) Representative images of western blotting for CDX2, S-I and KLF4 in AGS and BGC823 cells transfected as in Fig. 3A bottom. Right: Quantification of protein levels of CDX2, S-I and KLF4 respectively. β-actin levels were used as internal control. Means ± SEM of a representative experiment (n = 3) performed in triplicates are shown.*, $P < 0.05$; **, $P < 0.01$.

Figure S6

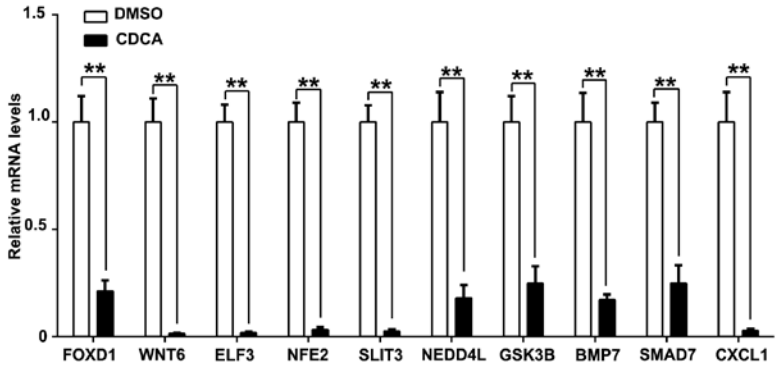

Supplemental Figure S6 Validation of whole genome expression profiles through qRT-PCR

Validation of mRNA levels of FOXD1, WNT6, ELF3, NFE2, NEDD4L, GSK3B, BMP7, SMAD7, CXCL1 in GES-1 cells treated with CDCA (100μM) for 24h as described in Fig. 1A. Means ± SEM of a representative experiment (n = 3) performed in triplicates are shown.*, $P < 0.05$; **, $P < 0.01$.

Figure S7

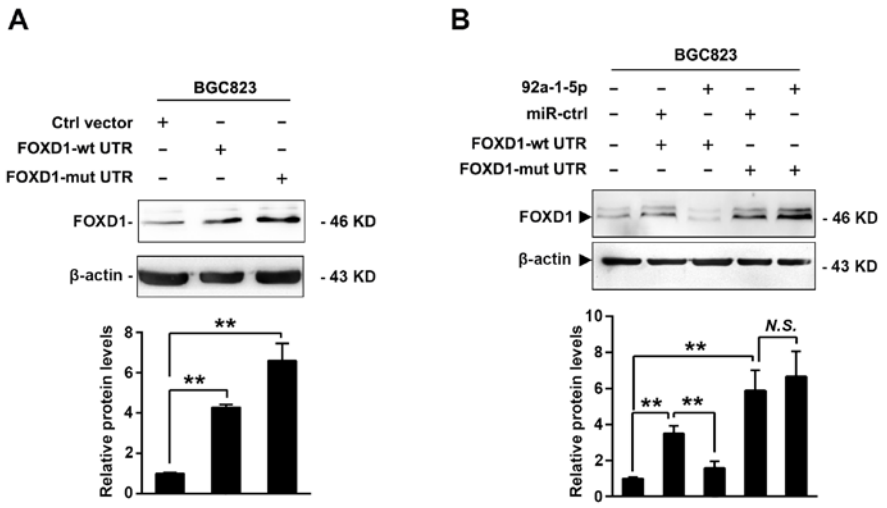

Supplemental Figure S7 miR-92a-1-5p targets FOXD1 3'UTR.

(A) Infection of FOXD1 expressing vectors with wild-type (wt) 3'-UTR or mutant (mut) 3'-UTR to BGC823 cells and FOXD1 expression were examined by immunoblot. (B) Lentiviral vectors with FOXD1 CDS and wt-UTR or mut-UTR were infected into BGC823 cells, followed by transfection of miR-92a-1-5p agomir. FOXD1 expressions were detected using western blot. Representative images in one of three independent experiments are shown. β-actin levels were used as internal control in immunoblots. Means ± SEM of a representative experiment (n = 3) performed in triplicates are shown.*, $P < 0.05$; **, $P < 0.01$.

Figure S8

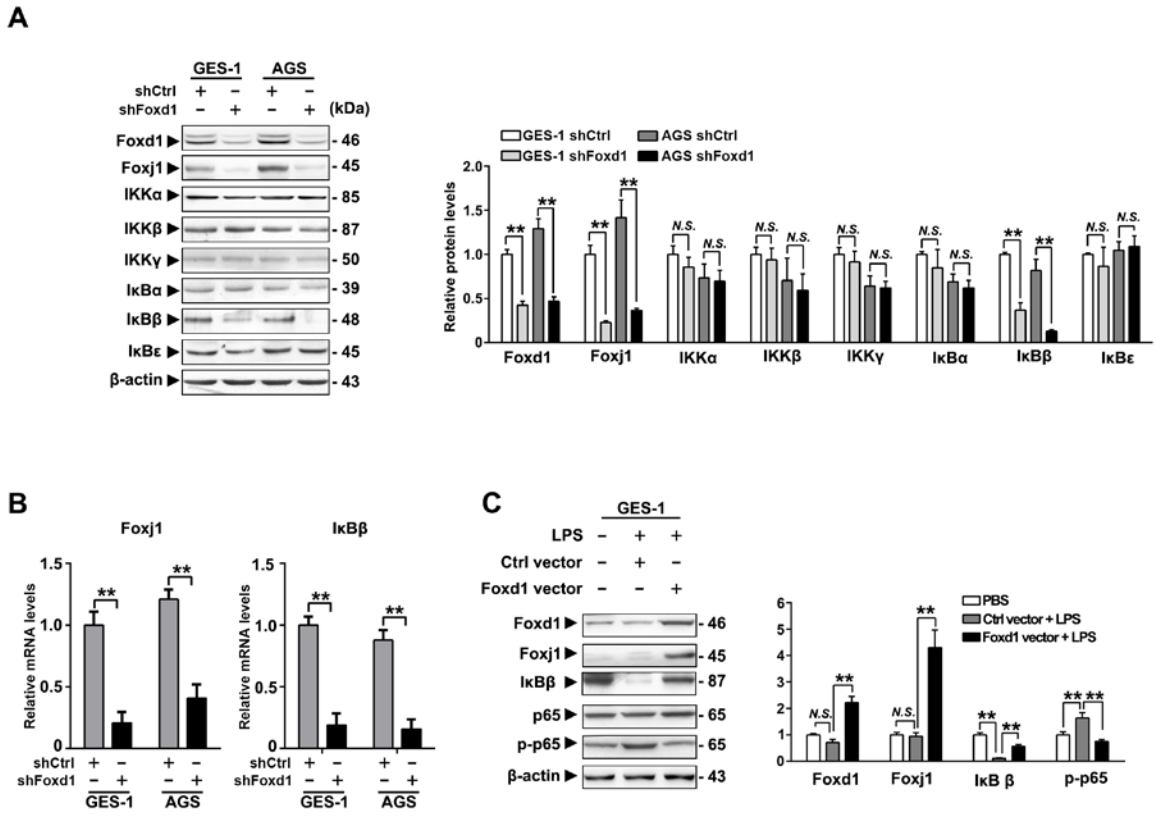

Supplemental Figure S8 FOXD1 positively regulates expression of FOXJ1 and IκBβ.

(A) Left: Representative images of western blotting showing knockdown of FOXD1 by shRNA led to decrease of protein levels of FOXJ1 and IκBβ in GES-1 and AGS cells, while expression IKKs and other IκBs were not affected. β-actin levels were used as internal control. Right: Quantification of immunoblotting results normalized as to β-actin. (B) qRT-PCR showed knockdown of FOXD1 by shRNA led to decrease of mRNA levels of FOXJ1 and IκBβ in GES-1 and AGS cells. GAPDH RNA was used as internal control. (C) GES-1 cells were infected with FOXD1-expressing vectors, and then treated with LPS (1μg/mL) for 4h. Western blotting showed restoration of FOXD1 partially abrogated LPS-induced decrease of IκBβ and activation of p65. Means ± SEM of a representative experiment (n = 3) performed in triplicates are shown.*, $P < 0.05$; **, $P < 0.01$.

Figure S9

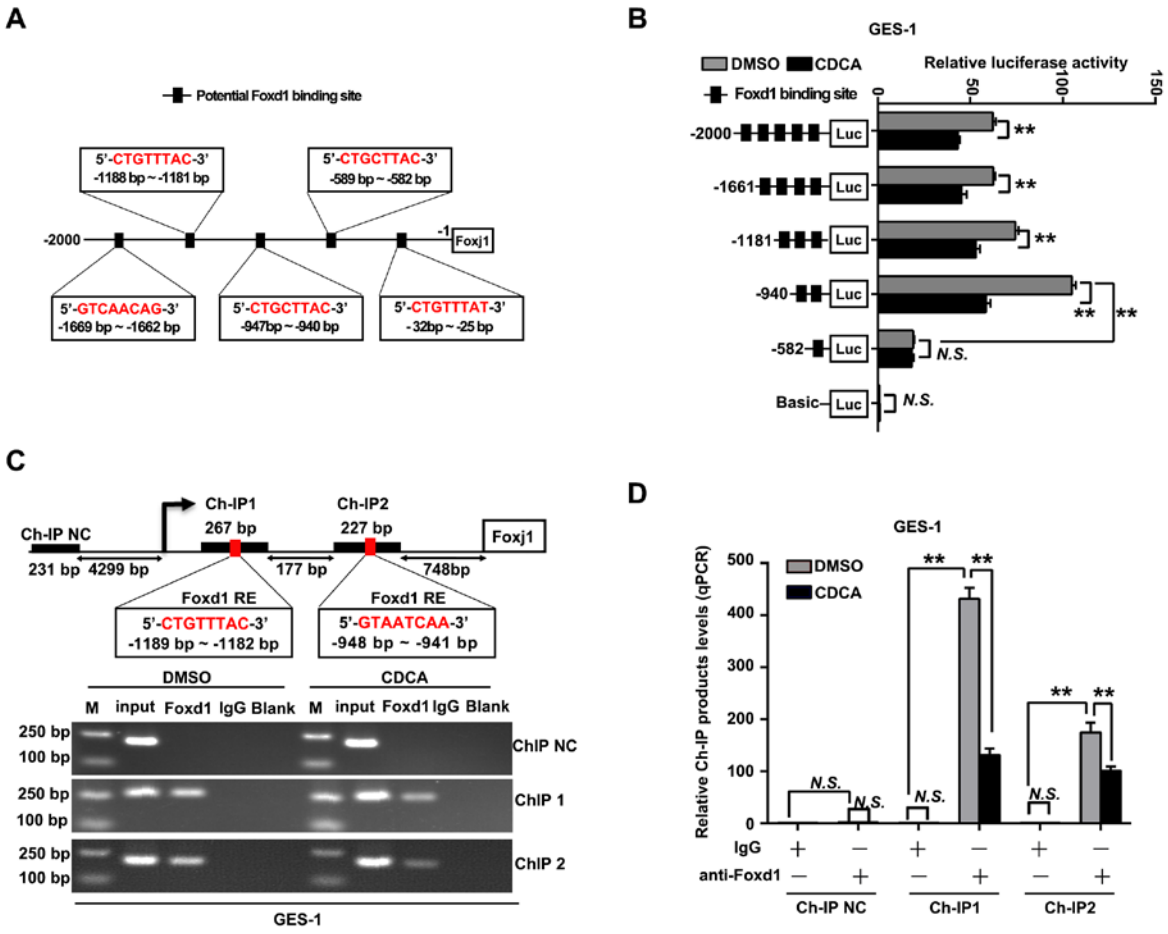

Supplemental Figure S9 FOXD1 promotes FOXJ1 transcription by binding to its promoter.

(A) A schematic representation of the FOXJ1 promoter containing 5 potential FOXD1 binding sites. (B) Serially truncated FOXJ1 promoter constructs were cloned to pGL3-luciferase reporter plasmids and transfected into GES-1 cells. 4h after transfection, cells were treated with CDCA (100μM) for 24h and the relative luciferase activities were determined 72h after ending of CDCA treatment. (C) A Ch-IP assay demonstrated the direct binding of FOXD1 to the FOXJ1 promoter in GES-1 cells. M: Marker. (D) qRT-PCR of the Ch-IP products validated the binding capacity of FOXD1 to the FOXJ1 promoter in GES-1 cells. Means ± SEM of a representative experiment (n=3) performed in triplicates are shown. *, $P < 0.05$; **, $P < 0.01$.

Figure S10

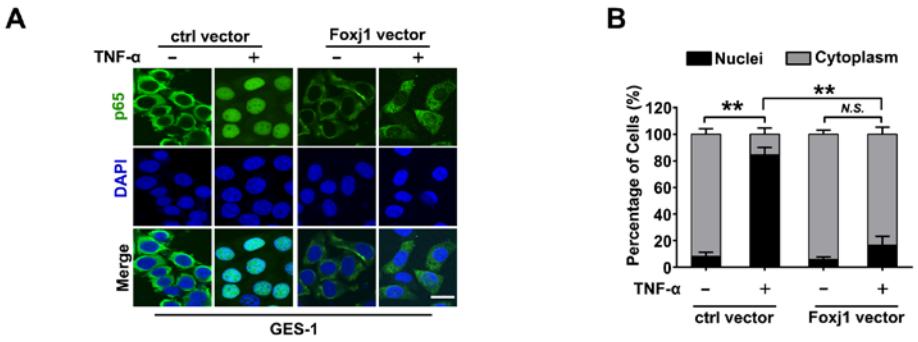

Supplemental Figure S10 FOXJ1 inhibits TNF-α-induced nuclear translocation of p65.

(A) Representative images of immunofluorescence analysis of p65 (green) in GES-1 cells while being treated with TNF-α (30 ng/mL) for 30 minutes. (F) Quantitation of p65 distribution in cells treated as in (B). Means ± SEM of a representative experiment (n=3) performed in triplicates are shown. *, $P < 0.05$; **, $P < 0.01$.

Figure S11

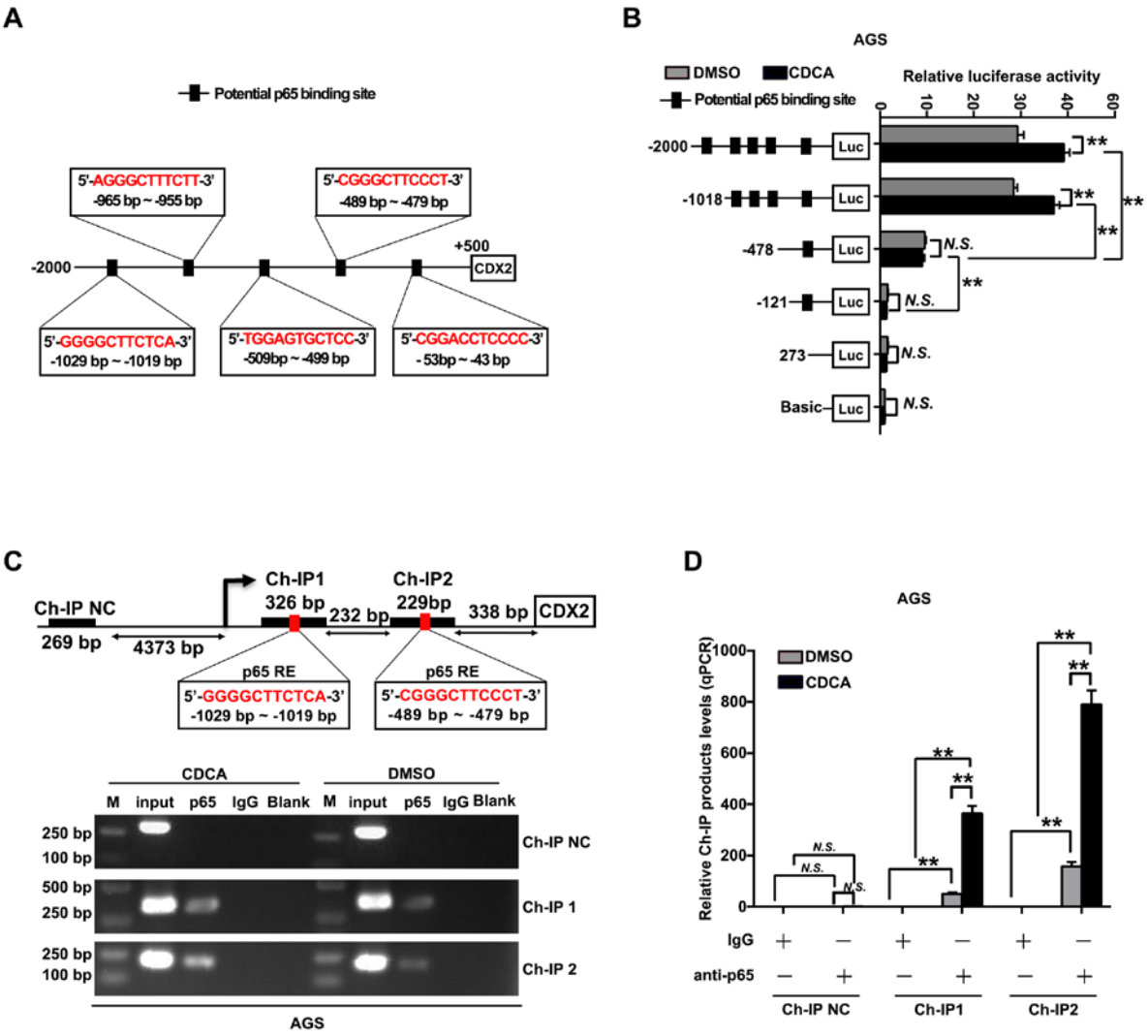

Supplemental Figure S11 NF-κB promotes CDX2 expression by directly binding to its promoter.

(A) A schematic representation of the CDX2 promoter containing 5 potential NF-κB binding sites. (B) Serially truncated CDX2 promoter constructs were cloned to pGL3-luciferase reporter plasmids and transfected into AGS cells. 4h after transfection, cells were treated with CDCA (100μM) for 24h and the relative luciferase activities were determined 24h after ending of CDCA treatment. (C) A Ch-IP assay demonstrated the direct binding of p65 to the CDX2 promoter in AGS cells. M: Marker. (D) qRT-PCR of the Ch-IP products validated the binding capacity of p65 to the CDX2 promoter in AGS cells. Means ± SEM of a representative experiment (n = 3) performed in triplicates are shown.*, $P < 0.05$; **, $P < 0.01$.